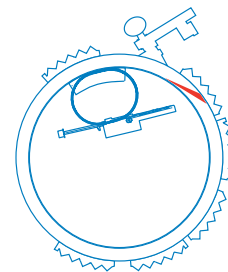# X-RAY IMAGING & MICROSPECTROSCOPY OF THE MYCORRHIZAL FUNGUS-PLANT SYMBIOSIS

ZHONGHOU CAI[*], WENBING YUN[*], STEPHEN T. PRATT,[†] RAYMOND M. MILLER[†],
EFIM GLUSKIN[*], DOUGLAS B. HUNTER[‡], AMIEL G. JARSTFER[§], KENNETH M. KEMNER[†],
BARRY LAI[*], HEUNG-RAE LEE[*], DANIEL G. LEGNINI[*], WILLIAM RODRIGUES[*],
& CHRISTOPHER I. SMITH[†]

*Experimental Facilities Division, Argonne National Laboratory • †Environmental Research Division, Argonne National Laboratory • ‡Savannah River Ecology Laboratory, The University of Georgia • §LeTourneau University

The scanning microprobe (right) at beamline 2-ID-D joins the high brilliance of an Advanced Photon Source undulator source to the high performance of a phase zone plate as a microfocusing device. The microprobe is demonstrating unprecedented submicron spatial resolving power that can be used in a wide range of x-ray applications. A focal spot of less than 0.25 μm (FWHM) has been demonstrated, and a photon flux density exceeding $5 \times 10^{10}/sec/\mu m^2/0.01\%BW$ has been obtained. The microprobe can simultaneously perform x-ray diffraction microscopy, fluorescence microscopy, spectromicroscopy, and 3D tomography with submicron spatial resolution. It has been used for a broad range of applications since commissioning in December of 1996, including the study of plant roots and fungi (described in this article), platinum-based anti-cancer agents, integrated laser/modulator microdevices, electromigration in Al wires in semiconductor devices, submicron spatial resolution and three-dimensional tomography of a single mammalian cell.

X-ray fluorescence microscopy (XFM) and microspectroscopy with unprecedented capabilities at micron spatial resolution have been developed on the 2-ID-D/E hard x-ray beamline at the Advanced Photon Source (APS) and applied to the study of the symbiotic relationship between mycorrhizal fungi and plants. These new capabilities for the study of biological and environmental samples couple high-brilliance synchrotron radiation and high-performance x-ray microfocusing optics to the intrinsic advantages of x-rays for element mapping and chemical-state imaging.

Approximately 90% of the world's vascular plants, including the majority of all economic crops, belong to families that commonly have symbiotic associations with mycorrhizal fungi.[1,2] While such associations are known to increase plant viability under low nutrient conditions, in some instances mycorrhizal fungi can also moderate toxicity effects in plants growing in soils containing elevated concentrations of heavy metals.[3,4] Thus, an improved understanding of the plant-fungus relationship, particularly with respect to the uptake mechanisms for metals, is expected to have significant implications in both agriculture and the remediation and restoration of contaminated environments.

X-ray fluorescence microscopy and microspectroscopy can provide information on the spatial distribution, oxidation state, chemical environment, and chemical transformations of trace elements.[5-10] In comparison with electron and proton microprobes,[10] the cross sections of x-ray fluorescence excited by x-rays are typically 10 to 10^3 times higher than those excited by charged particles, and the

fluorescence signal-to-background ratios are 10 to 10^5 times better for excitation by x-rays. Although the spatial resolution of electron and proton microprobes can approach molecular dimensions and is better than that achievable with x-rays, the elemental sensitivity is limited to approximately 100 ppm for electron-induced x-ray microanalysis and 10 ppm for proton-induced x-ray microanalysis, considerably worse than with x-rays.[11] In addition, the energy deposition for x-rays is 10^3 to 10^5 times smaller for a given elemental detectability,[10] resulting in substantially less radiation damage to the sample. Moreover, sample preparations for x-ray microprobes are far simpler than those for charged-particle microprobes, making it possible to study samples in their natural hydration states, which is not possible using charged-particle microprobes. With charged-particle microprobes, the samples must be stained and thinned to improve both contrast and signal-to-noise ratio, coated with a thin conducting layer to reduce charging effects and improve spatial resolution, and be in vacuum to maintain the charged-particle beams. Finally, information on the chemical state of the detected elements is difficult to obtain using techniques based on charged particles.

In recent years, soft x-ray (<1 keV) microscopy and spectromicroscopy have been successfully used for the study of biological samples.[5] However, higher energy x-rays are required to access the K edge of the third-row and heavier elements in the periodic table, many of which are either important nutrients, micronutrients, or contaminants with potentially toxic effects. The fluorescence yield for high-energy x-rays is also significantly greater than that for soft x-rays (it can be much less than 1%), and hard x-rays suffer considerably less attenuation along the optical path to and from the sample. The improvement in hard x-ray imaging and microspectroscopy techniques is expected to have important implications for the study of biological and environmental systems.

The high brilliance of third-generation synchrotron sources and developments in microfabrication technologies for high-resolution and high-efficiency hard x-ray zone plates[12] have resulted in substantial advances in the state of the art in x-ray spectromicroscopy, fluorescence microscopy, and phase contrast imaging. In this article, we report recent experimental results, obtained at the 2-ID-D/E beamline of the APS,[13] illustrating these capabilities by hard x-ray phase contrast imaging, XRF imaging, and microspectroscopy of mycorrhizal plant roots and fungi in their natural hydrated states. The XRF microprobe is demonstrated by the simultaneous mapping of the elemental distributions of P, S, K, Ca, Mn, Fe, Ni, Cu, and Zn with a spatial resolution of approximately 1x3 μm and
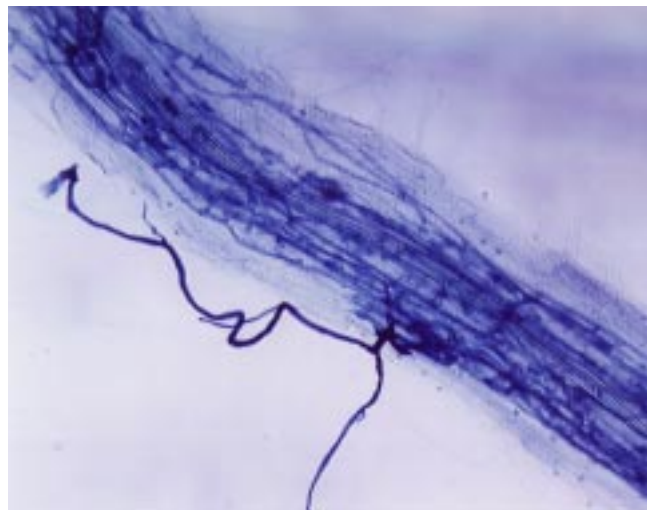

FIG 1(a). *An optical micrograph of a clarified and stained* P. lanceolata *root infected by the mycorrhizal fungus* Glomus mosseae.

with an elemental sensitivity of approximately 10 ppb. Microspectroscopy with the same spatial resolution is demonstrated by recording near-edge x-ray absorption (XANES) spectra of Mn at a concentration of approximately 3 ppm. These results specifically address the uptake mechanisms of metals by mycorrhizal plants and fungi.

An optical micrograph of a *Plantago lanceolata L.* root that has been infected by the arbuscular mycorrhizal fungus *Glomus mosseae* is shown in Fig. 1(a). X-ray phase contrast imaging provides a particularly effective method for imaging the sample and locating suitable regions of interest for fluorescence mapping and micro-XANES measurements. Phase contrast images were recorded by using a combination of scintillation crystal and charge-coupled-device detector system. Because the absorption contrast of the root-fungus sample at the x-ray energy (11.9 keV) used in the experiments is essentially invisible, the phase change when the x-rays pass through the sample provides the main contrast for the image. Figure 1(b) shows a phase contrast image of a hydrated plant root infected with the mycorrhizal fungus. The dark structure through the center of the root is a well-formed stele, which is indicative of the hydrated state of the root. A phase contrast image of an air-dried root (not shown) shows a shriveled and collapsed stele. The threadlike features coming off approximately perpendicular to the root are fungal hyphae. The hyphae can be distinguished from root hairs because they branch and enter the root at multiple points.
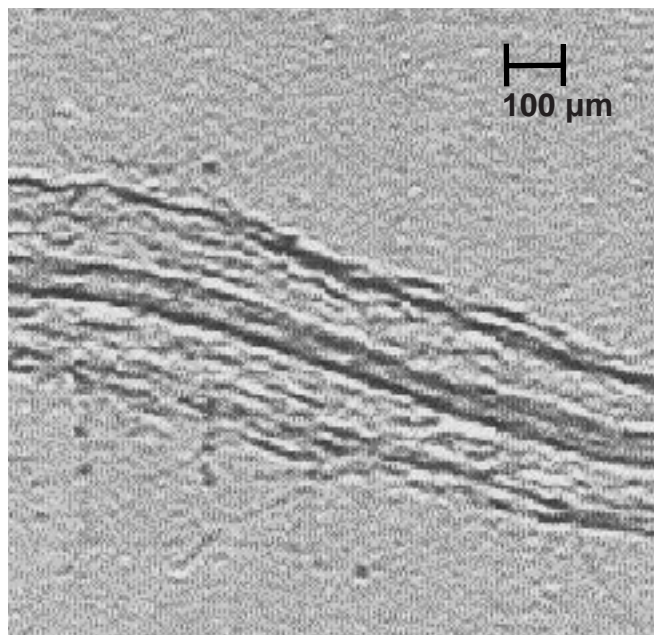
FIG. 1(b). A hard x-ray phase contrast image of an unclarified, unstained, wet P. lanceolata *root infected by the mycorrhizal fungus* Glomus mosseae.

The spatial resolution of the images in Fig. 1(a) and 1(b) is comparable; as a point of reference, an average root cell is approximately 80 mm in length and 30 mm in diameter. Similar features are observed in the optical and phase contrast images. It must be stressed, however, that the optical image of Fig. 1(a) required substantial sample preparation, while the phase contrast image of Fig. 1(b) required essentially none and could even be applied to living plants. Thus, the phase contrast image shows structures that could be lost or altered in the preparation of the sample for optical imaging. Nevertheless, a more detailed comparison of optical images and hard x-ray phase contrast images is expected to be informative, especially when the phase contrast images are recorded near the K edges of selected elements of interest, which will provide some elemental selectivity. The simplicity and short exposure times of the phase contrast method make it an extremely useful tool for positioning the sample for XRF imaging and microspectroscopy.

The XRF-imaging and microspectroscopy experiments were performed using a focused x-ray beam of 11.9 keV, with a zone plate of $1 \, \mu m$ x $3 \, \mu m$ cross section and 3×10^{10} photons/s/0.01% BW. A schematic of the beamline apparatus is shown in Fig 2. Samples for the XRF images were mounted at 45° to the incident beam, and the 3-μm-wide horizontal beam projected on the sample $4.2 \, \mu m$ approximately while the $1 \, \mu m$ vertical dimension of the beam was preserved. In order to take advantage of the polarization of the synchrotron radiation and to reduce the background, x-ray fluorescence from the sample was monitored at 90° to the incident beam horizontally by using an energy-dispersive detector. The integrated intensities of the Kα fluorescence corresponding to individual elements were measured as functions of the sample's vertical and horizontal positions with $5 \, \mu m$ steps and collection time of 3 seconds for each point. Although this means that the image was somewhat under sampled in the vertical dimension, this step size was necessary to image the desired regions of the sample with reasonable data-acquisition times. The total data-collection time for a 61 x 61 pixel array (300 x 300 μm^2) was approximately 4 h.

Figure 3 shows a series of images of a wet fungus sample analyzed for the micronutrients Mn, Fe, Cu, and Zn. Similar images have been recorded for the nutrients P, K, S, Ca, and Ni. The absolute element concentrations were determined by calibrating the detector with standard films. The nutritional requirements for elements can be divided into two concentration classes: macronutrients, required at about 10^{-3} M, and micronutrients, required at 10^{-6} M or less.[2] The macronutrients measured in this study were P, K, S, and Ca; the micronutrients were Fe, Mn, Cu, Zn. We also measured Ni, a metal normally considered toxic at high concentrations.

The distributions of the four micronutrients in Fig. 3 show different behavior. Interestingly, there is little evidence for Mn in the fungal hyphae, which may be related to the observation that mycorrhizal plants typically have much lower Mn concentrations than non-mycorrhizal plants.[2] The Fe tends to be most concentrated at the edge of the root, perhaps reflecting the precipitation of Fe in this location. Both Cu and Zn show up most strongly in the fungal hyphae and in the center of the root, most likely in the inner cortex where the proliferation of the fungus is greatest (see Fig. 1[a]). This suggests the use of Cu and Zn as surrogate measures of mycorrhizal fungi in roots.

With only a few exceptions, images of even completely dried roots show features similar to those in the hydrated root of Fig. 3. One striking contrast between the dry and wet samples is the significantly smaller amount of K in the fungal hyphae of the dried sample. Although the present results do not indicate whether the K moves into the root or to the outside of the hyphae, the mobilization of K upon drying of the sample could have important implications in the development of remediation technologies. More specifically, fungi are particularly effective in taking up Cs from soils, and their use in the sequestration and removal of radioactive Cs from contaminated sites has been discussed.[14] If Cs, like K, is mobilized upon drying, the effectiveness of the remediation strategy could be compromised. Efforts to characterize Cs uptake and mobility are

currently under way. The observations for K also illustrate the potential of the x-ray imaging techniques described here for the study of dynamical and transport processes in biological systems.

Although the XRF images of Fig. 3 provide detailed information on the spatial distributions of selected elements, they provide no information on the chemical states or local environments of the elements. To further demonstrate the capabilities of the x-ray microprobe, we recorded micro-x-ray absorption near-edge structure (XANES) spectra at the Mn K edge with a 1 x 3 μm spot size at a selected area within the sample shown in Figs. 1(b) and 2. Mn is an essential micronutrient in both plants and fungi, and in natural systems it usually exists in the +2 or +4 oxidation state (the +3 oxidation state is also possible but generally unstable). The +2 oxidation state is soluble and is the form that is most useful to plants and fungi.[2] The +4 oxidation state is insoluble and has less biological importance. The small beam size used in these experiments ensured that a single fungal hypha can be studied if desired.

The XANES spectra were obtained by positioning an interesting feature of the sample in the focused x-ray beam and scanning the x-ray energy through the absorption edge while monitoring the Mn Kα fluorescence. Figure 4 shows a Mn micro-XANES spectrum with the beam aligned to the stele in the center of the root. Each point in the spectrum was averaged for 10 s of detector live time, and the full spectrum was recorded in approximately 45 min. The spectrum has been normalized by the intensity of the transmitted light. XANES spectra were recorded in a variety of locations across the sample, including the root cortex and the extramatrical fungal hyphae. In this sample, the Mn XANES spectrum was found to be independent of position, and all of the spectra were essentially indistinguish-able from the one in Fig. 4. (Spectra on the fungal hyphae were somewhat noisier as a result of the small amount of hyphal material.) Comparison of our results with detailed XANES studies of a wide variety of samples and standards[15,16] indicated that at least 90% of the Mn sampled by the x-ray beam at each of the locations is Mn^{+2}. This is clear from the sharp rise at threshold and the relatively intense white line, as opposed to the gradual onset and weak white line observed in Mn^{+4}. Although the observation of Mn^{+2} in the present sample is not surprising, the results demonstrate the ability to record high-quality XANES spectra with 1 x 3 μm spatial resolution. In principle, similar measurements for other third-row and heavier elements should be straightforward.

The combination of high-brilliance synchrotron radiation from the APS and high-performance zone plates provides substantial improvements in the state of the art of hard x-ray phase contrast imaging, XRF imaging, and micro-XANES spectroscopy of biological and environmental samples. Hard x-ray phase contrast imaging was shown here to provide a straightforward, sensitive, high-resolution method for imaging biological samples with minimal radiation damage. XRF imaging at the APS can now be performed with monochromatic radiation, resulting in a substantial reduction in background due to scattered radiation. New zone plates should soon allow element-specific, hard x-ray XRF imaging with submicron spatial resolution. Although the benefits to phase contrast imaging and XRF imaging are substantial, perhaps the most striking advance is the decrease by a factor of approximately 100 in the beam size. This makes microspectroscopy techniques useful for gathering information on the chemical states and local environments of elements on a scale compatible with a
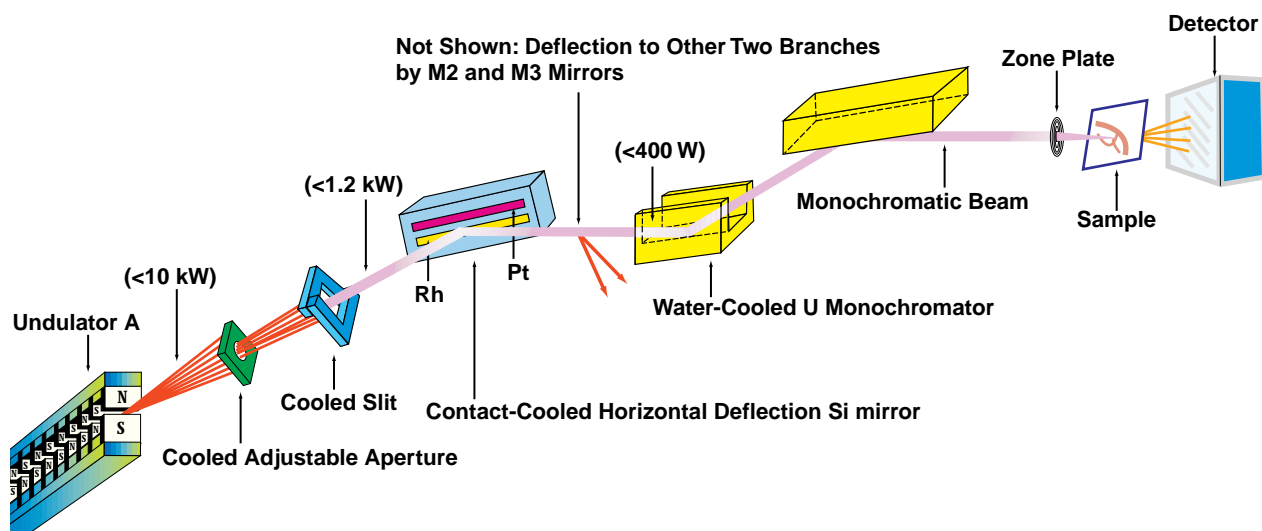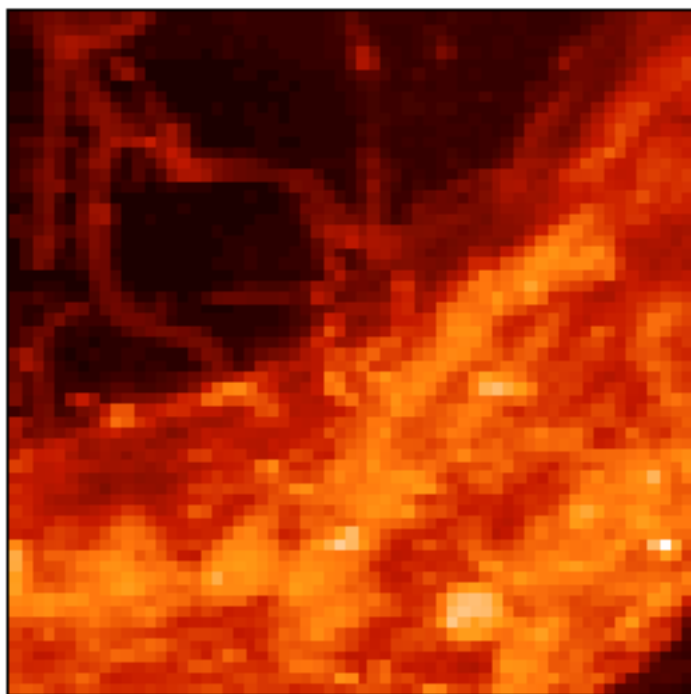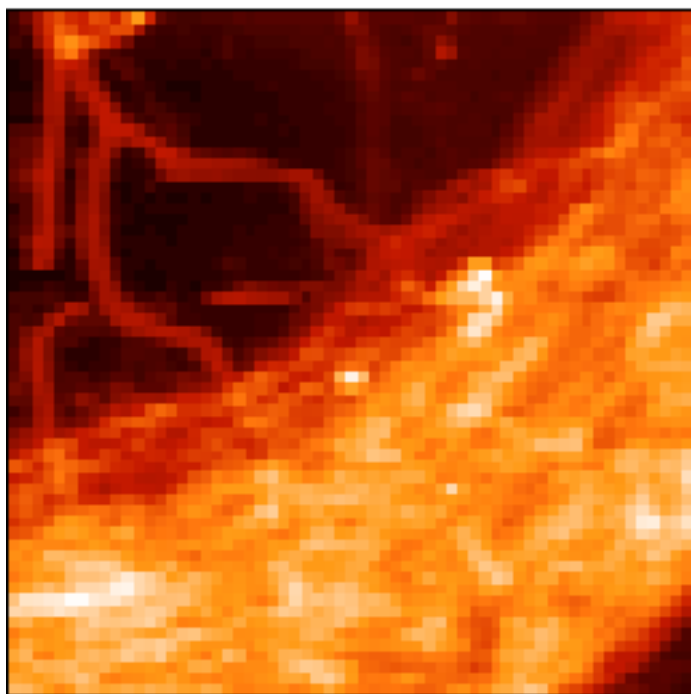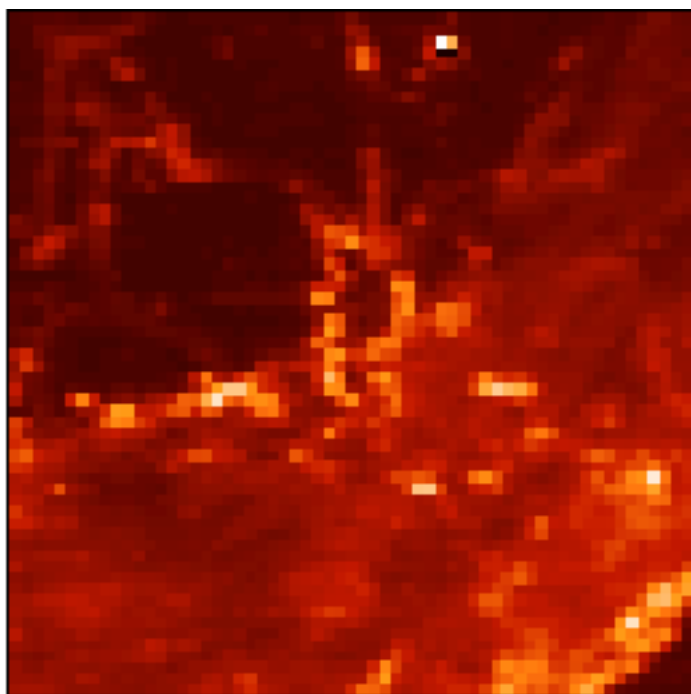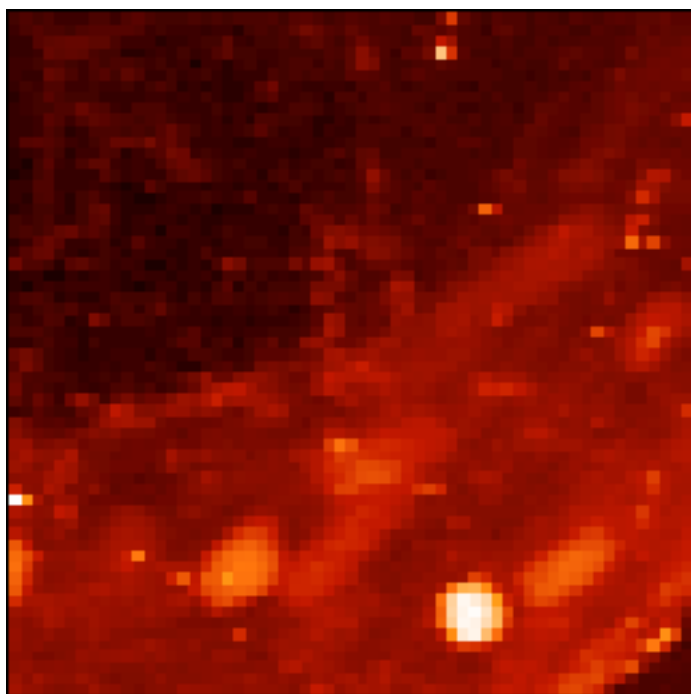
FIG. 2. One of three branches on the 2-ID D/E - Sector 2, insertion device branch line.

Mn: 0.03 to 0.87 µg/cm²

Fe: 0.11 to 27.9 µg/cm²

Cu: 0.03 to 1.55 µg/cm²

Zn: 0.04 to 4.98 µg/cm²

300x300 µm area
5x5 µm pixels

Min. Max.

FIG. 3. Selected element–specific XRF images of a hydrated P. lanceolata *root infected by the mycorrhizal fun-gus* G. mosseae. *This is a portion of the root shown in the phase contrast image in Fig. 1(b).*
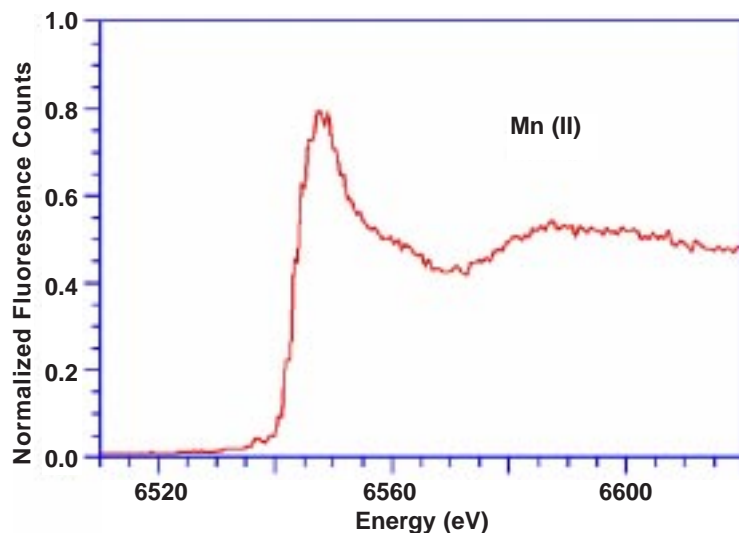
FIG. 4. The micro-XANES spectrum at the Mn K edge obtained with a 1 μm x 3 μm focal spot aligned to the stele in the central portion of the root shown in Fig. 1(b). Comparison of the spectrum with known standards indicates that at least 90% of the Mn is in the +2 oxidation state.

variety of important biological and cellular structures. The commissioning of new imaging beamlines at the APS and other third-generation synchrotron sources is expected to result in a rapid development of capabilities to address issues in the biological and environmental sciences. ❍

REFERENCES

[1] M. F. Allen, *The Ecology of Mycorrhizae* (Cambridge University Press, New York, 1991).

[2] H. Marschner, *Mineral Nutrition of Higher Plants*, Second Edition (Academic Press, New York, 1995).

[3] R. Bradley, A. J. Burt, and D. J. Read, Nature **292**, 335 (1981); R. Bradley, A. J. Burt, and D. J. Read, New Phytol. **91**, 197 (1982).

[4] U. Galli, H. Schüepp, and C. Brunold, Physiol. Plantarum **92**, 364 (1994).

[5] J. Kirz, C. Jacobsen, and M. Howells, Quart. Rev. Biophys. **28**, 33 (1995).

[6] S. V. Mattigod, M. L. Rivers, and S. R. Sutton, in *Synchrotron X-Ray Sources and New Opportunities in the Soil and Environmental Sciences: Workshop Report*, edited by D. G. Schulze and J. V. Smith, Argonne National Laboratory Report ANL/APS/TM-7, 101 (July 1990).

[7] D. G. Schulze and P. M. Bertsch, Adv. Agron. **55**, 1 (1995).

[8] P. M. Bertsch, D. B. Hunter, S. R. Sutton, S. Bajt, and M. L. Rivers, Environ. Sci. Technol. **28**, 980 (1994).

[9] See, for example, D. C. Koningsberger and R. Prins, *X-Ray Absorption: Principles, Applications, Techniques of EXAFS, SEXAFS, and XANES* (Wiley, New York, 1988).

[10] C. J. Sparks, Jr., in *Synchrotron Radiation Research*, edited by H. Winick and S. Doniach (Plenum Press, New York, 1980) p. 459.

[11] B. Forslind, K. G. Malmquist, and J. Pallon, Scanning Microscopy **5**, 877 (1991).

[12] B. Lai, W. Yun, D. Legnini, Y. Xiao, J. Chrzas, P.J. Viccaro, V. White, S. Bajikar, D. Denton, and F. Cerrina, App. Phys. Lett. **61**, 1877 (1992).

[13] W. Yun, B. Lai, D. Shu, A. Khounsary, Z. Cai, J. Barraza, and D. Legnini, Rev. Sci. Instrum. **67, (9)** CD-ROM.

[14] K. Haselwandter, M. Berreck, and P. Brunner, Trans. Br. Mycol. Soc. **90**, 171 (1988); G. M. Clint, J. Dighton, and S. Rees, Mycol. Res. **95**, 1047 (1991); J. Dighton, G. M. Clint, and J. Poskitt, Mycol. Res. **95**, 1052 (1991).

[15] D. G. Schulze, T. McCay-Buis, S. R. Sutton, and D. M. Huber, Phytopathol. **85**, 990 (1995); D. G. Schulze, S. R. Sutton, and S. Bajt, Soil Sci. Soc. Am. J. **59**, 1540 (1995).

[16] A. Manceau, A. I. Gorshkov, and V. A. Drits, Am. Mineralogist **77**, 1133 (1992); A. Manceau, A. I. Gorshkov, and V. A. Drits, Am. Mineralogist **77**, 1144 (1992).